Transverse spin and energy flow in Kerker scattering

Zhaolou Cao [1,2] and Chunjie Zhai [3,*]

[1] *Jiangsu International Joint Laboratory on Meteorological Photonics and Optoelectronic Detection, Nanjing University of Information Science and Technology, Nanjing 210044, China*

[2] *Jiangsu Key Laboratory for Optoelectronic Detection of Atmosphere and Ocean, Nanjing University of Information Science and Technology, Nanjing 210044, China*

[3] *Department of Information Technology, Nanjing Police College, Nanjing 210046, China*

(Received 30 April 2023; revised 4 December 2023; accepted 23 January 2024; published 14 February 2024)

In this paper, we investigate the characteristics of transverse spin and energy flow in Kerker scattering by a high refractive-index nanosphere based on the rigorous Mie scattering theory. It is found that the spin is quasi-transverse to the direction of energy flow everywhere in Kerker scattering and the magnitude of transverse spin is much larger than that in Rayleigh scattering due to the phase shift between scattered light of electric and magnetic dipoles. For the incidence of a linearly polarized plane wave, the transverse spin predominantly determines the direction of energy flow due to the spin-momentum locking effect in the near field. In the far field, the curl relationship between the energy flow and spin angular momentum density is validated analogously to structured guided waves. These findings help deepen understandings of unidirectional scattering and will be beneficial for the design of photonic nanoantennas.

DOI: 10.1103/PhysRevA.109.023518

I. INTRODUCTION

Light scattering by small particles is of fundamental significance in a wide range of physics, such as astronomy, imaging, climate studies, etc. Despite it is an old topic, novel scattering phenomena and theories are still emerging fostered by the flourishing field of photonics nowadays. In recent years, controlling the angular distribution of scattered light by a particle has been a hot topic in the optics community, of which unidirectional scattering has attracted a lot of attention for its potential applications in nanoantennas [1,2], particle positioning with subatomic precision [3], and photovoltaic devices [4]. In 1983, Kerker *et al.* [5] found that the backward scattering by a magnetic sphere is strongly suppressed under some conditions, namely, Kerker's conditions of equal permittivity and permeability, where the scattered light of electric (ED) and magnetic dipoles (MD) with the same amplitude cancels each other out in the backward direction through destructive interference. Several approaches [6–8] were proposed to steer the direction of scattered light since Kerker's work. Whereas most natural materials possess weak magnetism, materials with high refractive indices or engineered metamaterials provide a platform for exotic light manipulation through the interference of multipole modes.

On the other hand, there has been growing interest in light beams carrying spin angular momentum (SAM) and orbit angular momentum (OAM). At subwavelength scales, many optical phenomena, such as propagation, diffraction, and focusing, are affected by the spin-orbit interactions of light. A lot of work has been devoted towards connections between optical spin and momentum [9–11], showing that the conversion between SAM and OAM can be achieved by several methodologies, such as the tight focusing of light by a high-numerical-aperture lens system [12] and scattering by a small particle or aperture [13]. In these works, it was demonstrated that the spin direction may be transverse to the propagation direction in coherent and incoherent structured beams [14–17] while it is along the propagation direction for paraxial beams. The transverse spin has an intrinsic relationship with the energy flow, known as the optical spin-to-momentum locking effect. Recently, Yuan and co-workers proved that the transverse spin and energy flow can be arranged in a form analogous to Maxwell's equation for structured guided waves, showing that there is a curl relationship between transverse spin and energy flow [18]. This type of transverse spin was also observed in light scattering by particles. Saha *et al.* [19] studied the evolution of SAM of light scattered by a sphere from the near field to far field. Triolo *et al.* [20] systematically analyzed the spin-momentum locking effect in the near field of metal particles supporting localized surface resonances. These works are a direct manifestation of extraordinary transverse spin of evanescent waves in the near field of scattered light, raising the question of how the transverse spin influences the energy flow of Kerker scattering. In this paper, the characteristics of transverse spin and energy flow of Kerker scattering by a high refractive-index nanosphere in the far and near fields are investigated based on the rigorous Mie scattering theory. The results presented here will help deepen the understandings of spin controlled unidirectional scattering.

II. THEORY

The schematic of the scattering problem is shown in Fig. 1. A high refractive-index nanoparticle assumed to be a sphere located in an x-polarized plane wave propagating in the z direction scatters light in different directions. According to

*Corresponding author: zhaichunjie1988@163.com

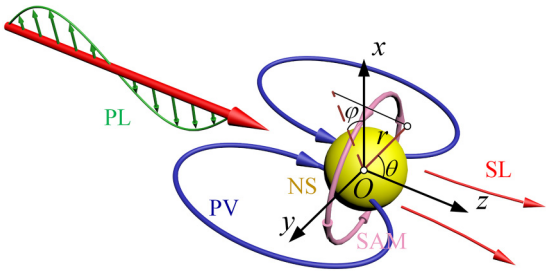

FIG. 1. Schematic of unidirectional scattering of an x-polarized beam by a high refractive-index nanosphere. PL: polarization; PV: Poynting vector; NS: nanosphere; SL: scattered light; SAM: spin angular momentum. The Cartesian coordinate system (x, y, z) is attached to the sphere and its origin is located at the sphere center. The corresponding spherical system (r, θ, φ) is used throughout the following text.

the Mie scattering theory, the scattered light for a spherical particle in an x-polarized plane wave is given by

$$\mathrm{E}_s = \sum_{n=1}^{\infty} E_n\left[ia_n \mathrm{N}_{e|n}^{(3)} - b_n \mathrm{M}_{o|n}^{(3)}\right], \tag{1}$$

$$\mathrm{H}_s = \frac{1}{Z_0}\sum_{n=1}^{\infty} E_n\left[a_n \mathrm{M}_{e|n}^{(3)} + ib_n \mathrm{N}_{o|n}^{(3)}\right] \tag{2}$$

in the spherical coordinate system following the notations of Bohren and Huffman [21], where $Z_0 = (\mu_0/\varepsilon_0)^{1/2}$ is the vacuum impedance, ε_0 and μ_0 respectively stand for the permittivity and permeability of vacuum, $E_n = i^n E_0(2n+1)/n(n+1)$, E_0 denotes the electric field amplitude, $\mathbf{M}$ and $\mathbf{N}$ denote vector spherical harmonics, and a_n and b_n are conventional Mie scattering coefficients. Detailed expressions of the six components $[E_r, E_\theta, E_\varphi, H_r, H_\theta, H_\varphi]$ of the nth term of electromagnetic field in the spherical coordinate system of (r, θ, φ) are given in Appendix A.

The SAM ($\mathbf{S}$) of a three-dimensional electromagnetic field including the contribution of both electric and magnetic fields is given by

$$\mathrm{S} = \frac{1}{4\omega}\mathrm{Im}[\varepsilon_0 \mathrm{E}* \times \mathrm{E} + \mu_0 \mathrm{H}* \times \mathrm{H}], \tag{3}$$

where $\omega = 2\pi c/\lambda$; c is the light speed and λ is the wavelength.

Since we focus on scattering by nanoparticles much smaller than the wavelength, only a_1 associated with an ED and b_1 associated with a MD to need be considered. In the far field of conventional Mie scattering, it is well known that the SAM should be along the direction of Poynting vector like a plane wave or spherical wave even when the radial components of E_r and H_r are taken into account. However, it is different for Kerker scattering, where $a_1 = b_1$. In this case, Eqs. (A3)–(A8) can be simplified to

$$E_r = 2E_1 a_1 \cos\varphi \ \sin\theta \frac{-ie^{ikr}}{(kr)^2}, \tag{4}$$

$$E_\theta = E_1 a_1 \cos\varphi \frac{e^{ikr}}{kr}(\cos\theta + 1), \tag{5}$$

$$E_\varphi = -E_1 a_1 \sin\varphi \frac{e^{ikr}}{kr}(\cos\theta + 1). \tag{6}$$

$$H_r = \frac{2E_1 a_1}{Z_0} \sin\varphi \ \sin\theta \frac{-ie^{ikr}}{(kr)^2}, \tag{7}$$

$$H_\theta = \frac{E_1}{Z_0} a_1 \sin\varphi \frac{e^{ikr}}{kr}(\cos\theta + 1), \tag{8}$$

$$H_\varphi = \frac{E_1 a_1}{Z_0} \cos\varphi \frac{e^{ikr}}{kr}(\cos\theta + 1) \tag{9}$$

in the far field, where $k = 2\pi/\lambda$, r is the propagation distance, and the spherical Hankel function of the first order is asymptotically expressed as

$$h_1^{(1)}(\rho) = \frac{-e^{i\rho}}{\rho}, \tag{10}$$

$$\frac{dh_1^{(1)}(\rho)}{d\rho} = \frac{-ie^{i\rho}}{\rho} \tag{11}$$

in the far field ($\rho \to \infty$).

It can be figured out that the electric field is linearly polarized in the transverse plane when the radial component (E_r) is not considered, as $E_\theta/E_\varphi = -\cos\varphi/\sin\varphi$ is a real number. Similar expressions can be obtained for the magnetic field. Since there is a phase delay of $\pi/2$ between E_r and transverse components (E_θ and E_φ) analogous to the evanescent wave in the total reflection of a plane wave at a planar interface, the direction of SAM is always perpendicular to the propagation direction except at the singularity in the backward direction, demonstrating that the spin is always transverse in the far field.

To account for the impact of inhomogeneous SAM on the energy flow [20], an additional spin momentum is required to be introduced into the Poynting vector in the Mie scattering problem. The energy flow $\mathbf{p} = \mathbf{P}/c^2$, where $\mathbf{P} = \mathrm{Re}(\mathbf{E} \times \mathbf{H}^*)/2$ is the Poynting vector and c is the light speed, can be decomposed into two parts: one for the contribution of orbital energy flow density ($\mathbf{p}^{\mathrm{o}}$) and the other for the contribution of spin momentum density ($\mathbf{p}^{\mathrm{s}}$), given by

$$\mathbf{p} = \mathbf{p}^{\mathrm{o}} + \mathbf{p}^{\mathrm{s}}, \tag{12}$$

$$\mathrm{p}^o = \frac{1}{4\omega}\mathrm{Im}[\varepsilon_0 \mathrm{E}* \cdot(\boldsymbol{\nabla})\mathrm{E} + \mu_0 \mathrm{H}* \cdot(\boldsymbol{\nabla})\mathrm{H}], \tag{13}$$

$$\mathrm{p}^{\mathrm{s}} = \frac{1}{2}\boldsymbol{\nabla} \times \mathrm{S}. \tag{14}$$

It was recently demonstrated that there is a curl relationship between energy flow and transverse spin with a form analogous to Maxwell's equation for several structured guided modes [18], such as cosine beam, Bessel beam, Weber beam, and Airy beam. While Eq. (14) indicates the inhomogeneity of SAM produces a spin momentum, the inhomogeneity of energy flow leads to transverse SAM, given by

$$\boldsymbol{\nabla} \times \mathrm{p} = 2k^2 \mathrm{S}_t, \tag{15}$$

where the subscript t denotes the transverse component. Since the SAM is transverse in the far field of Kerker scattering, the validity of the curl relationship was examined analytically.

Substituting Eqs. (4)–(9) into Eq. (15), one obtains

$$\begin{aligned}\mathbf{p} &= \mathrm{Re}(\mathbf{E}\times\mathbf{H}^*)/c^2\\ &= \mathrm{Re}\left[E_\theta H_\varphi^* - E_\varphi H_\theta^* E_\varphi H_r^* - E_r H_\varphi^* E_r H_\theta^* - E_\theta H_r^*\right]/c^2\\ &= \left[\frac{E_1^2|a_1|^2}{Z_0 c^2 k^2 r^2}(\cos\theta+1)^2 00\right], \end{aligned} \tag{16}$$

$$\nabla\times\mathbf{p} = \frac{2E_1^2|a_1|^2}{Z_0 c^2 k^2 r^3}[00(\cos\theta+1)\sin\theta], \tag{17}$$

and

$$\begin{aligned}\mathrm{S} &= \frac{\varepsilon}{4\omega}\mathrm{Im}[E_\theta^* E_\varphi - E_\varphi^* E_\theta E_\varphi^* E_r - E_r^* E_\varphi E_r^* E_\theta - E_\theta^* E_r] + \frac{\mu}{4\omega}\mathrm{Im}[H_\theta^* H_\varphi - H_\varphi^* H_\theta H_\varphi^* H_r - H_r^* H_\varphi H_r^* H_\theta - H_\theta^* H_r]\\ &= \frac{\varepsilon}{\omega}\frac{E_1^2|a_1|^2}{k^3 r^3}[00\sin\theta(\cos\theta+1)]. \end{aligned} \tag{18}$$

After substituting $\omega = kc$ and $\varepsilon = \frac{1}{Z_0 c}$ into Eq. (26), the curl relationship is validated. The results suggest that the scattered light in the far field of Kerker scattering is similar to structured guided waves to some extent. It was conjectured that transverse spin is pervasive in a structured light field and originates from the inhomogeneities (intensity, phase, polarization) [18]. In the case of Kerker scattering in the far field, the energy flow given by Eq. (16) is along the radial direction but inhomogeneous along the polar direction in the far field. As a result of the curl relationship, the inhomogeneity indicates the rotation of polarization and hence transverse spin along the azimuthal direction, which requires a phase shift of E_r with respect to E_θ and E_φ. The analysis can also be applied to a separate ED or MD, where the light is linearly polarized in the transverse plane. For a more general case of Mie scattering ($a_1 \neq b_1$), the phase shift between a_1 and b_1 produces longitudinal spin with a magnitude much larger than that of transverse spin. As Eq. (15) works only for the transverse spin, the curl relationship is not valid for the scattered light in a general Mie scattering problem. Nevertheless, Eq. (23) offers a convenient approach to distinguish transverse and longitudinal SAM in the total SAM.

III. RESULTS AND DISCUSSION

In the near field, the radial components of electric and magnetic fields may have much larger magnitudes than those of transverse components, resulting in different phenomena of SAM and energy flow from that in the far field. For a nanoparticle with a relative permeability approximating to 1, the magnitude of b_1 is much smaller than that of a_1. In this case, the scattering problem can be reduced to Rayleigh scattering, where the forward and backward scattering determined by the ED have nearly the same magnitude. In order to achieve unidirectional scattering by destructive interference, a high permeability is required to increase the magnitude of b_1.

Without loss of generality, we considered the scattering of an x-polarized plane wave with $[E_x, E_y, E_z] = [10^{10}, 0, 0]$ by a nanosphere with a radius of 20 nm, refractive index of 3.5, and relative permeability of 3.5 in the air. The results for Kerker scattering [Figs. 2(a) and 2(b)] are compared with those of Rayleigh scattering by a nanosphere with the same radius and refractive index, but relative permittivity of 1, which can be approximated as an ED [Figs. 2(c) and 2(d)]. In the far field of Kerker scattering, the radial and azimuthal components of electric field vanish, while the magnitude of polar component decreases gradually with the increase of θ, as shown in Fig. 2(a). As expected, the electric field is zero in the backward direction. Meanwhile, the near-field light field shows a more complicated pattern in Fig. 2(b). At $\theta = 90^\circ$, the radial and polar components respectively have the maximum and minimum magnitude. As the two components are symmetric to $\theta = 90^\circ$, there is no sign of the far-field directional scattering in the near field. By comparison, polar components of electric fields show the same pattern in the near and far fields for Rayleigh scattering in Figs. 2(c) and 2(d). As the radial component is nearly zero in the far field, a quasi-symmetry to the xOz plane is observed in the near field

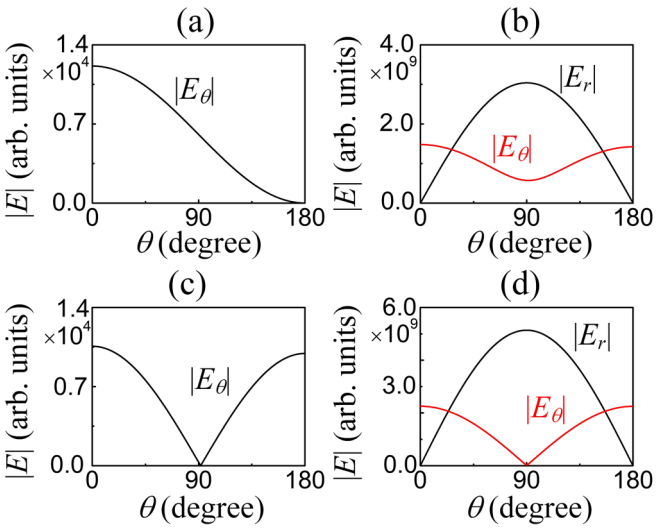

FIG. 2. Scattering of a nanosphere with a relative permeability of 3.5: (a) far-field electric field magnitude in the xOz plane ($r = 1$ mm, $\varphi = 0^\circ$), $E_r = 0$, $E_\varphi = 0$. (b) Near-field electric field magnitude in the xOz plane ($r = 30$ nm, $\varphi = 0^\circ$), $E_\varphi = 0$. (c) and (d) are the same as (a) and (b), but for a nanosphere with a relative permeability of 1.

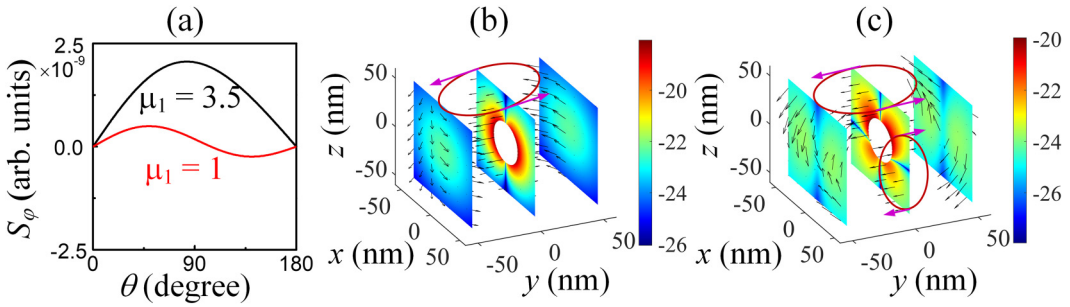

FIG. 3. (a) The azimuthal component of SAM density at $r = 30$ nm in the xOz plane. Three-dimensional SAM distribution in the near field of (b) Kerker and (c) Rayleigh scattering. The SAM inside the particle is not plotted and the color bar shows the logarithmic value of SAM magnitude. The arrow direction represents the SAM direction, while the arrow length is set to be the fourth root of SAM magnitude for better illustration of direction. A hard threshold of $e^{-8}S_{\max}$ is applied to avoid the singularity of zero SAM for the logarithmic calculation, where $S_{\max}$ is the maximum value of SAM magnitude.

like that in the far field, indicating that the near-field energy flow of Kerker scattering should be quite different from that of Rayleigh scattering.

Although the incident plane wave is linearly polarized, the elliptically polarized scattered light reveals a nonzero SAM. The SAM of Kerker and Rayleigh scattering are compared in Fig. 3. The SAM should be transverse in the xOz plane since the azimuthal component of electric field is zero. Due to the phase retardation of electromagnetic field between the ED and MD, the maximum magnitude of $|S_\varphi|$ for $\mu_1 = 3.5$ is much higher than that for $\mu_1 = 1$. As the electric and magnetic contribution to the radial (polar) component cancel each other, the SAM should be along the azimuthal direction [see Appendix B and Eq. (18)]. While S_φ does not change its sign between 0° and 180° in Kerker scattering, it appears as a sinusoidal curve and is 0 at $\theta = 105°$ in Rayleigh scattering, exhibiting two additional zero-SAM points in the side direction. Note that the exact direction of the two additional zero-SAM points varies with the propagation, which changes from 105 ° at $r = 30$ nm to 97° at $r = 45$ nm to 95° at $r = 60$ nm and forms two zero-SAM curves. The variation originates from the superposition of the MD, although its magnitude is much smaller than that of the ED. The difference in the existence of zero-SAM points produces a significant difference in the three-dimensional SAM distribution in the near field of Kerker and Rayleigh scattering, as shown in Figs. 3(b) and 3(c). The SAM magnitude decreases rapidly with the propagation since it is significantly affected by the radial component of electric field. As optical vortices at zero-SAM points indicate the change of SAM direction, the SAM only rotates about the z axis in Kerker scattering, while it rotates about both the z-axis and zero-SAM curves in the side direction in Rayleigh scattering.

The intrinsic optical spin-momentum locking effect is then examined in the near field of Mie scattering. Figure 4 shows the energy flow, decomposed into spin and orbit components, at $r = 30$ nm from the sphere center. The negative value of the radial component of energy flow at $\theta > 90°$ suggests that the energy does not necessarily spread out but may spread towards the sphere center in Fig. 4(a). The far-field scattered light is thus weak in the backward direction. As the polar component of energy flow is always non-negative, the energy flows from the forward direction to the backward direction outside the sphere. It can be found that the energy flow is predominantly determined by its spin component in Kerker scattering, where the spin and orbit components are generally in the opposite direction. As the scattered light propagates into the far field, the spin components gradually attenuate and the energy flow is mainly determined by its orbit component in the far field, which is validated but not explicitly given in a figure. A similar explanation can be made for Rayleigh scattering. The counteraction between spin and orbit components leads to a weak energy flow in Figs. 4(c) and 4(d), where the radial component is positive in the forward direction and negative in the backward direction. This type of energy flow results in a slightly lower intensity of scattered light in the backward direction than that in the forward direction, as shown in Fig. 2(c). Therefore, transverse spin plays an important role in reshaping the energy flow in the near field of light scattering.

Figure 5 gives the three-dimensional energy flow in the near field of Kerker and Rayleigh scattering. In Kerker scattering [Figs. 5(a)–5(c)], the direction of energy flow generally agrees with that of the spin component, which is towards

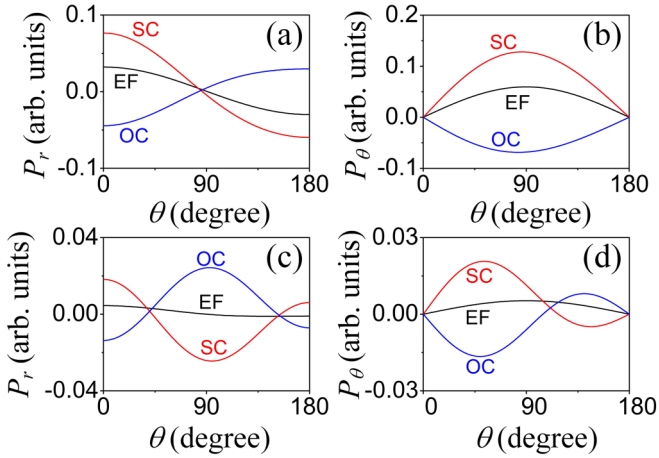

FIG. 4. (a) Radial and (b) polar components of the energy flow at $r = 30$ nm in the xOz plane for $\mu_1 = 3.5$. (c) and (d) are the same as (a) and (b) but for $\mu_1 = 1$. The azimuthal component is zero for both Kerker scattering and Rayleigh scattering. SC: spin component; OC: orbit component; EF: energy flow.

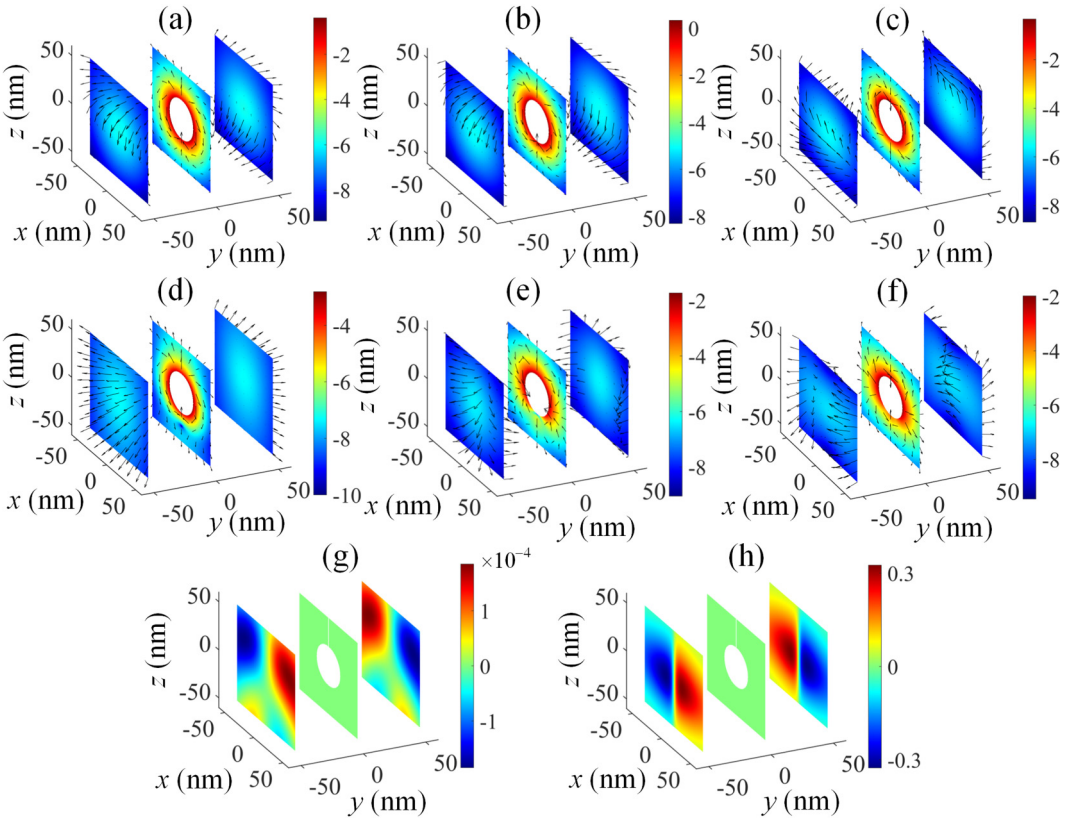

FIG. 5. Three-dimensional energy flow in the near field: (a) energy flow, (b) spin component, and (c) orbit component for Kerker scattering; (d), (e), and (f) are the same as (a), (b), and (c), but for Rayleigh scattering. The color bar shows the logarithmic value of the magnitude of energy flow and its component. The arrow direction and length are plotted in the same manner as that in Fig. 3. The direction cosine between SAM and Poynting vector for (g) Kerker scattering and (h) Rayleigh scattering.

the backward direction. Due to the contribution of MD, the energy flow of Kerker scattering is quite different from that of a spherical wave in the region of $100 \times 100 \times 100$ nm. By comparison, the energy flows in the same manner as that of a spherical wave in Rayleigh scattering at the boundary of the region in Fig. 5(d). According to the spin-momentum locking effect, the direction of energy flow should be perpendicular to that of localized transverse SAM. However, it may not work in the near field of light scattering as the scattered light is a mixture of evanescent and propagating waves. The direction cosine, denoted as α, between two vectors, denoted as $\mathbf{V}_1$ and $\mathbf{V}_2$, is employed as a metric to quantitatively characterize the angle between SAM and energy flow, given by

$$\alpha = \frac{\mathbf{V}_1 \cdot \mathbf{V}_2}{\|\mathbf{V}_1\|\|\mathbf{V}_2\|}. \tag{19}$$

The spatial distribution of direction cosine between SAM ($\mathbf{V}_1$) and Poynting vector ($\mathbf{V}_2$) is given in Figs. 5(g) and 5(h). The maximum of absolute direction cosine is 1.8×10^{-4} at $y = \pm 50$ nm in Kerker scattering and 0.33 at $y = \pm 50$ nm in Rayleigh scattering. The near-zero direction cosine indicates that the SAM direction is approximately perpendicular to the energy flow in the near field of Kerker scattering. In contrast, the scattered light is linearly polarized and the energy flow is always along the radial direction in the near field for a single ED (see Appendix B). As the scattered light is the superposition of that of ED and MD, the difference between Kerker scattering and Rayleigh scattering originates from the influences of the MD. According to Eqs. (B3)–(B8), the phase shift of light from ED and MD is $\pi/2$ for both polar and azimuthal components in the near field of Kerker scattering. In this case, the SAM and the energy flow are perpendicular to each other due to the spin-momentum locking effect (see Appendix B). The energy flow [Eq. (B12)] can be naturally decomposed into two parts: one flows outside towards the radial direction [the second term on the right-hand side of Eq. (B12)] and the other is highly confined in the near field [the first term on the right-hand side of Eq. (B12)]. It is interesting to find that the curl relationship in Eq. (15) is valid for the energy flow going outside and SAM. Considering the SAM is always transverse in the far field of Kerker scattering, it can be concluded that the spin is quasi-transverse everywhere in Kerker scattering. It should be mentioned that the conclusion is only valid for the incidence of a linearly polarized plane wave.

IV. CONCLUSION

In conclusion, we investigate the energy flow and transverse spin in the near and far fields of Kerker scattering and find several interesting features. The superposition of ED and MD with the same magnitude significantly reduce the magnitude of longitudinal SAM in Kerker scattering compared

with that of Rayleigh scattering. Due to the spin-momentum locking effect, the energy flow is reshaped to steer the angular distribution of scattered light. It is further demonstrated that in Kerker scattering, the spin is quasi-transverse to the Poynting vector in both the near and far fields. The present study helps deepen the understanding of unidirectional scattering, and the results can be conducive to exploring novel mechanisms and designing nanoantennas.

ACKNOWLEDGMENTS

This work was supported by the National Natural Science Foundation of China (Grants No. 52106162 and No. 61605081) and the Qing Lan Project, the Priority Academic Program Development of Jiangsu Higher Education Institutions of China.

Z.C. conducted the simulation and wrote the manuscript. C.Z. conceptualized the work, and wrote and edited the draft.

The authors declare that they have no known competing financial interests or personal relationships that could have appeared to influence the work reported in this paper.

APPENDIX A

In Eqs. (1) and (2), the Mie scattering coefficients are expressed as

$$a_n = \frac{\mu m^2 j_n(mx)[x j_n(x)]' - \mu_1 j_n(x)[mx j_n(mx)]'}{\mu m^2 j_n(mx)\left[x h_n^{(1)}(x)\right]' - \mu_1 h_n^{(1)}(x)[mx j_n(mx)]'}, \quad \text{(A1)}$$

$$b_n = \frac{\mu_1 j_n(mx)[x j_n(x)]' - \mu j_n(x)[mx j_n(mx)]'}{\mu_1 j_n(mx)\left[x h_n^{(1)}(x)\right]' - \mu h_n^{(1)}(x)[mx j_n(mx)]'}, \quad \text{(A2)}$$

where $j_n(x)$ and $h_n^{(1)}(x)$ are respectively the spherical Bessel and spherical Hankel functions, m is the relative refractive index, $x = kr_0$, $k = 2\pi/\lambda$ is the wave number, r_0 is the particle radius, and μ and μ_1 are respectively the relative permeability of the surrounding medium and particle. The six components of the nth term of electromagnetic field in the spherical coordinate system of (r, θ, φ) can then be obtained as

$$E_r = iE_n a_n \cos\varphi n(n+1)\sin\theta \pi_n(\cos\theta)\frac{h_n^{(1)}(kr)}{kr}, \quad \text{(A3)}$$

$$E_\theta = iE_n a_n \cos\varphi \tau_n(\cos\theta)\frac{\left[kr h_n^{(1)}(kr)\right]'}{kr} - E_n b_n \cos\varphi \pi_n(\cos\theta) h_n^{(1)}(kr), \quad \text{(A4)}$$

$$E_\varphi = -iE_n a_n \sin\varphi \pi_n(\cos\theta)\frac{\left[kr h_n^{(1)}(kr)\right]'}{kr} + E_n b_n \sin\varphi \tau_n(\cos\theta) h_n^{(1)}(kr), \quad \text{(A5)}$$

$$H_r = \frac{iE_n b_n}{Z_0}\sin\varphi n(n+1)\sin\theta \pi_n(\cos\theta)\frac{h_n^{(1)}(kr)}{kr}, \quad \text{(A6)}$$

$$H_\theta = i\frac{E_n b_n}{Z_0}\sin\varphi \tau_n(\cos\theta)\frac{\left[kr h_n^{(1)}(kr)\right]'}{kr} - \frac{E_n a_n}{Z_0}\sin\varphi \pi_n(\cos\theta) h_n^{(1)}(kr), \quad \text{(A7)}$$

$$H_\varphi = \frac{iE_n b_n}{Z_0}\cos\varphi \pi_n(\cos\theta)\frac{\left[kr h_n^{(1)}(kr)\right]'}{kr} - \frac{E_n a_n}{Z_0}\cos\varphi \tau_n(\cos\theta) h_n^{(1)}(kr), \quad \text{(A8)}$$

where special angular functions $\pi_n(\cos\theta) = \frac{P_n^{(1)}(\cos\theta)}{\sin\theta}$ and $\tau_n(\cos\theta) = \frac{dP_n^{(1)}(\cos\theta)}{d\theta}$ are defined using associated Legendre polynomials $P_n^{(1)}(\cos\theta)$ for convenience.

APPENDIX B

In the near field ($\rho \to 0$), the spherical Hankel function of the first order is asymptotically expressed as

$$h_1^{(1)}(\rho) = \frac{-i}{\rho^2}, \quad \text{(B1)}$$

$$\frac{dh_1^{(1)}(\rho)}{d\rho} = 0.5 + \frac{2i}{\rho^3}. \quad \text{(B2)}$$

The simplified light field is given by

$$E_r = 2E_1 a_1 \cos\varphi \sin\theta \frac{1}{(kr)^3}, \quad \text{(B3)}$$

$$E_\theta = -\frac{E_1\cos\varphi}{(kr)^2}\left(\frac{a_1\cos\theta}{kr} - ib_1\right), \quad \text{(B4)}$$

$$E_\varphi = \frac{E_1\sin\varphi}{(kr)^2}\left(\frac{a_1}{kr} - ib_1\cos\theta\right), \quad \text{(B5)}$$

$$H_r = \frac{2E_1 b_1}{Z_0}\frac{\sin\varphi\ \sin\theta}{(kr)^3}, \quad \text{(B6)}$$

$$H_\theta = -\frac{E_1}{Z_0}\frac{\sin\varphi}{(kr)^2}\left(\frac{b_1\cos\theta}{kr} - ia_1\right), \quad \text{(B7)}$$

$$H_\varphi = -\frac{E_1\cos\varphi}{Z_0(kr)^2}\left(\frac{b_1}{kr} - ia_1\cos\theta\right). \quad \text{(B8)}$$

For a single electric dipole ($b_1 = 0$), the SAM is zero since both the electric and magnetic fields are linearly polarized. Meanwhile, the Poynting vector $\mathbf{P} = \mathrm{Re}(\mathbf{E}\times\mathbf{H}^*)/2$ is almost purely imaginary, so the time-averaged energy flow is zero.

For Kerker scattering ($a_1 = b_1$), the scattered light is elliptically polarized with the orientation of major axis dependent on the position. The components of SAM and energy flow are expressed as

$$S_r = 0, \quad \text{(B9)}$$

$$S_\theta = 0, \quad \text{(B10)}$$

$$S_\varphi = \frac{\varepsilon_0|E_1 a_1|^2\sin\theta}{\omega(kr)^5}, \quad \text{(B11)}$$

$$p_r = \frac{|E_1 a_1|^2\cos\theta}{2Z_0 c^2(kr)^6} + \frac{|E_1 a_1|^2\cos\theta}{2Z_0 c^2(kr)^4}, \quad \text{(B12)}$$

$$p_\theta = \frac{|E_1 a_1|^2\sin\theta}{Z_0 c^2(kr)^6}, \quad \text{(B13)}$$

$$p_\varphi = 0. \quad \text{(B14)}$$

While the SAM is always along the azimuthal direction, the energy flows towards the radial and polar directions. While SAM and the energy flow are still perpendicular to each other, the curl relationship in Eq. (15) is not valid. However, it is found that the curl relationship does exist between the SAM and part of the energy flow, viz.,

$$\nabla \times \mathrm{p} = 2k^2 \mathrm{S}, \tag{B15}$$

where $\mathbf{p} = [p_{r2}, 0, 0]$, $\mathbf{S} = [0, 0, S_\varphi]$, and p_{r2} is the second term on the right-hand side of Eq. (B12).

[1] P. D. Terekhov, H. K. Shamkhi, E. A. Gurvitz, K. V. Baryshnikova, A. B. Evlyukhin, A. S. Shalin, and A. Karabchevsky, Broadband forward scattering from dielectric cubic nanoantenna in lossless media, Opt. Express **27**, 10924 (2019).

[2] M. F. Picardi, A. V. Zayats, and F. J. Rodríguez-Fortuño, Janus and Huygens dipoles: Near-field directionality beyond spin-momentum locking, Phys. Rev. Lett. **120**, 117402 (2018).

[3] A. Bag, M. Neugebauer, P. Woźniak, G. Leuchs, and P. Banzer, Transverse Kerker scattering for angstrom localization of nanoparticles, Phys. Rev. Lett. **121**, 193902 (2018).

[4] H. A. Atwater and A. Polman, Plasmonics for improved photovoltaic devices, Nat. Mater. **9**, 205 (2010).

[5] M. Kerker, D. S. Wang, and C. L. Giles, Electromagnetic scattering by magnetic spheres, J. Opt. Soc. Am. **73**, 765 (1983).

[6] K. Matsushima, Y. Noguchi, and T. Yamada, Unidirectional invisibility in a PT-symmetric structure designed by topology optimization, Opt. Lett. **47**, 3315 (2022).

[7] Y. Yu, J. Liu, Y. Yu, D. Qiao, Y. Li, and R. Salas-Montiel, Broadband unidirectional transverse light scattering in a V-shaped silicon nanoantenna, Opt. Express **30**, 7918 (2022).

[8] L. Liu, J. Shen, and Z. Li, Tuning magneto-electric coherent resonance with a deep-subwavelength localized spoof surface plasmonic structure, Opt. Lett. **48**, 855 (2023).

[9] K. Y. Bliokh and F. Nori, Transverse and longitudinal angular momenta of light, Phys. Rep. **592**, 1 (2015).

[10] K. Y. Bliokh, F. J. Rodríguez-Fortuño, F. Nori, and A. V. Zayats, Spin-orbit interactions of light, Nat. Photonics **9**, 796 (2015).

[11] M. Antognozzi, C. R. Bermingham, R. L. Harniman, S. Simpson, J. Senior, R. Hayward, H. Hoerber, M. R. Dennis, A. Y. Bekshaev, K. Y. Bliokh, and F. Nori, Direct measurements of the extraordinary optical momentum and transverse spin-dependent force using a nanocantilever, Nat. Phys. **12**, 731 (2016).

[12] Y. Zhao, D. Shapiro, D. Mcgloin, D. T. Chiu, and S. Marchesini, Direct observation of the transfer of orbital angular momentum to metal particles from a focused circularly polarized Gaussian beam, Opt. Express **17**, 23316 (2009).

[13] C. Schwartz and A. Dogariu, Conservation of angular momentum of light in single scattering, Opt. Express **14**, 8425 (2006).

[14] J. X. Guo, W. Y. Wang, T. Y. Cheng, and J. Q. Lü, Interaction of spin-orbit angular momentum in the tight focusing of structured light, Front. Phys. **10**, 1079265 (2022).

[15] J. Chen, L. Yu, C. Wan, and Q. Zhan, Spin–orbit coupling within tightly focused circularly polarized spatiotemporal vortex wavepacket, ACS Photonics **9**, 793 (2022).

[16] J. S. Eismann, L. H. Nicholls, D. J. Roth, M. A. Alonso, P. Banzer, F. J. Rodriguez-Fortuño, A. V. Zayats, F. Nori, and K. Y. Bliokh, Transverse spinning of unpolarized light, Nat. Photonics **15**, 156 (2021).

[17] J. Zhuang, L. Zhang, and D. Deng, Tight-focusing properties of linearly polarized circular Airy Gaussian vortex beam, Opt. Lett. **45**, 296 (2020).

[18] P. Shi, L. Du, C. Li, and X. Yuan, Transverse spin dynamics in structured electromagnetic guided waves, Proc. Natl. Acad. Sci. USA **118**, e2018816118 (2021).

[19] S. Saha, A. K. Singh, S. K. Ray, A. Banerjee, S. D. Gupta, and N. Ghosh, Transverse spin and transverse momentum in scattering of plane waves, Opt. Lett. **41**, 4499 (2016).

[20] C. Triolo, A. Cacciola, S. Patanè, R. Saija, S. Savasta, and F. Nori, Spin-momentum locking in the near field of metal nanoparticles, ACS Photonics **4**, 2242 (2017).

[21] C. F. Bohren and D. R. Huffman, *Absorption and Scattering of Light by Small Particles* (Wiley, New York, 1983).